Title

Cherenkov-type three-dimensional breakdown behavior of the Bloch-point domain wall motion in the cylindrical nanowire

Journal

Applied Physics Letters, 117(6)

ISSN

0003-6951

Authors

Ma, Xiao-Ping
Zheng, Jiangshan
Piao, Hong-Guang
et al.

Publication Date

2020-08-10

DOI

10.1063/5.0013002

Peer reviewed

Applied Physics Letters

Cherenkov-type three-dimensional breakdown behavior of the Bloch-point domain wall motion in the cylindrical nanowire

Cite as: Appl. Phys. Lett. **117**, 062402 (2020); https://doi.org/10.1063/5.0013002
Submitted: 08 May 2020 . Accepted: 24 July 2020 . Published Online: 11 August 2020

Xiao-Ping Ma, Jiangshan Zheng, Hong-Guang Piao, Dong-Hyun Kim, and Peter Fischer

Applied Physics Letters ARTICLE scitation.org/journal/apl

Cherenkov-type three-dimensional breakdown behavior of the Bloch-point domain wall motion in the cylindrical nanowire

Cite as: Appl. Phys. Lett. **117**, 062402 (2020); doi: 10.1063/5.0013002
Submitted: 8 May 2020 · Accepted: 24 July 2020 ·
Published Online: 11 August 2020

Xiao-Ping Ma,[1,2] Jiangshan Zheng,[1] Hong-Guang Piao,[1,a)] Dong-Hyun Kim,[2,3,4,a)] and Peter Fischer[4,5]

AFFILIATIONS

[1]Research Institute for Magnetoelectronis and Weak Magnetic-Field Detection, College of Science, China Three Gorges University, Yichang 443002, People's Republic of China
[2]Department of Physics, Chungbuk National University, Cheongju 28644, South Korea
[3]Research Institute for Nanoscale Science and Technology, Chungbuk National University, Cheongju 28644, South Korea
[4]Materials Sciences Division, Lawrence Berkeley National Laboratory, Berkeley, California 94720, USA
[5]Department of Physics, University of California at Santa Cruz, Santa Cruz, California 95064, USA

[a)]**Authors to whom correspondence should be addressed:** hgpiao@ctgu.edu.cn and donghyun@chungbuk.ac.kr

ABSTRACT

A three-dimensional breakdown behavior of the magnetic Bloch-point domain wall (BP-DW) propagation was investigated in a ferromagnetic nanowire with the variation of the external magnetic field by means of micromagnetic simulation. As magnetic field strength increases up to a threshold value, the BP-DW velocity approaches a critical phase velocity of the spontaneously emitting spin wave (SW), where a Cherenkov-type DW breakdown phenomenon is observed originating from an interaction between the spontaneously emitting SW and the BP-DW. It is found that the velocity of the BP-DW approaches a maximum value (∼2000 m/s) due to the intrinsic reversal time of a BP spin texture. This suggests that although cylindrical ferromagnetic nanowires might be free from the two-dimensional Walker breakdown phenomenon, there exists a Cherenkov-type three-dimensional breakdown behavior.

Recently, spin textures with a three-dimensional (3D) structure on various nanostructured magnetic systems have attracted much attention, motivated by stable 3D spin textures in topological solitons with topological charges such as vortices, skyrmions, hopfions, and chiral bobbers.[1–3] It has been suggested that such spin textures could be stabilized[4,5] or transformed with different topological charges[6,7] via formation and annihilation of a spin texture called the Bloch point (BP) with intrinsic 3D characteristics. It is expected that the BP plays an essential role in the dynamic nature of various spin textures; however, the associated spin dynamics that involves the BP has been elusive so far. The BP structure can be regarded as a 3D version vortex structure, where the magnetization circulates in all directions around the BP and is a strongly inhomogeneous magnetization singularity on an atomic length scale.[8–11] The BP can be easily generated in thicker ferromagnetic nanowires, with the thickness of more than a Bloch-wall width,[12] from the competition between exchange interaction and dipolar interaction, without requiring chiral interactions, such as Dzyaloshinskii–Moriya interaction.[11,13] For instance, in thicker cylindrical nanowires, the inner spin configuration of the magnetic domain wall (DW) is known to have a BP structure under proper conditions of a cylinder diameter and material parameters.[14–21]

In the case of 3D cylindrical nanowires, the DW driving mechanism and propagation behaviors significantly differ from the cases of two-dimensional (2D) flat nanowire. For the case of flat nanowires with a thin thickness whose thickness is less than a Bloch wall width, the transverse DW configuration becomes energetically favorable so that the driving mechanism by the external magnetic field is a torque built up between the external field and the demagnetizing field, where the demagnetizing field is formed by free poles, generated from the tilting magnetization of the transverse DW part,[22] on the wire plane. The driving torque becomes larger under a higher external magnetic field, resulting in a faster DW velocity. Numerous studies have been devoted to understanding the DW dynamics in various flat ferromagnetic

nanowires under the external magnetic field,[23–29] spin transfer torque,[30–35] propagating spin waves (SWs),[36–38] or spin–orbit torque.[39,40]

Based on numerous previous works, it has been also well known that transverse DWs keep the inner spin structure only under a relatively weak field. When the field is up to a threshold value, the inner spin structure exhibits a periodically transitional behavior between the transverse and the antivortex DWs, leading to a Walker breakdown behavior,[41] imposing a limit in applications since it makes the DW velocity relatively slow even under strong fields or high currents. The Walker breakdown behavior arises from overcoming the demagnetizing field in flat nanowires by the torque determined by the cross product between the external field and the magnetization of the transverse DW. It is interesting to note that the breakdown behavior is a geometry-dependent dynamic phenomenon,[29,42] which can be simply avoided, for instance, by adopting a cylindrically symmetric 3D nanowire. Indeed, for the transverse-like DW in a thin cylindrical soft Nickel nanowire with a diameter less than about 42 nm,[10,18] the spiral propagation behavior has been predicted with the absence of the Walker-like breakdown even under the high magnetic field.[10,43]

On the other hand, in a thicker cylindrical nanowire, the inner spin texture of the DW containing BP (BP-DW) is stabilized by allowing spin curling around the wire axis, minimizing the magnetostatic energy by suppressing the free pole generation on the wire surface.[20,44] The static BP-DW structure has been experimentally observed by high-resolution x-ray microscopy.[45] Recently, it has been numerically studied that there exists an intrinsic pinning behavior of the BP-DW although the pinning behavior remains questionable,[10] resulting in an onset field in BP dynamic motion under the external magnetic field,[20] which might be linked to the pinning on an atomic scale.[8,9] The intrinsic pinning behavior depends on the structure of DWs. In the 3D transverse-like DW of thinner cylindrical wires, it can be observed that the magnetic exchange energy between its internal spins is distributed relatively evenly. Therefore, there is no potential barrier/well that can prevent the DW from moving, as described in Ref. 43. However, the BP-DW is easily formed in thicker cylindrical wires, and the BP spin in the DW structure is bound by curling spins around it, which is accompanied by a large accumulation of exchange energy. Thus, not only the reversal behavior of BP spin is hindered, but also the initial DW movement is influenced to overcome this accumulated energy, effectively forming its intrinsic pinning, as described in Ref. 20. Phenomenologically, the onset behavior was ascribed to the inertial moment change of overall spin texture, which is energetically unfavorable in distorting the curling spin structure before shifting the BP itself. However, an important and interesting question naturally arises: if the BP can be effectively separated from the curling spin texture under a relatively high external field, will there be a new class of 3D BP-DW breakdown phenomena? Unfortunately, no study has been addressed to the BP dynamics under a high field so far, and no such breakdown behavior has been predicted. However, dynamic characteristics of the BP-DW require clear understanding since the BP dynamics is widely involved in creation, modification, and annihilation of the 3D spin textures.

In this Letter, we report micromagnetic simulations that show our finding that there exist a class of Cherenkov-type breakdown phenomena during the BP propagation along a cylindrical ferromagnetic nanowire, intrinsically arising from the 3D nature of the BP. During the breakdown, abrupt and substantial reduction of the BP-DW velocity is observed around a threshold external field. Although there is some similarity to the Walker breakdown in 2D, there are significant differences when going to 3D that have no counterpart in 2D. The breakdown occurs via the faster-moving BP, exceeding the propagation velocity of the curling spin texture, so that the BP structure emits SWs analogous to the Cherenkov radiation. Although there are some debates on the BP behavior,[10,11] it brings abundant new phenomena to the study of micromagnetism. Our finding based on a basic magnetic interaction provides a fundamental point of view in understanding of BP dynamics involved with other chiral interactions.

The dynamic behavior of the BP-DW in a ferromagnetic cylindrical nanowire was investigated by means of micromagnetic simulations.[46,47] In the simulation, a soft ferromagnetic nanowire is considered with Permalloy material parameters, where the saturation magnetization is $M_s = 8.6 \times 10^5$ A/m, the exchange stiffness coefficient is $A = 13 \times 10^{-12}$ J/m, the Gilbert damping constant is $\alpha = 0.01$, and the magnetocrystalline anisotropy is set to be zero to better reveal the effect of shape characteristics of the cylindrical nanowire. A cylindrical nanowire of 2-μ m length is considered with a diameter of 50 nm, as illustrated in the schematic of Fig. 1(a). The total effective calculation volume of the cylindrical nanowire is discretized into 312 500 cells with a unit cell size of $4 \times 2 \times 2$ nm^3, where a 2×2 nm^2 grid mesh is on the cross-sectional (yz) plane of the nanowire and the 4-nm grid size is along the nanowire axis (x) direction. To investigate the BP-DW propagation behavior in the cylindrical nanowire, a head-to-head BP-DW of the right-handed chirality is positioned at the nanowire center as the starting configuration to stabilize the DW dynamic behavior,[10,48,49] and its chirality is a combination of the DW clockwise-curled spin structure and the field direction. Figure 1(b) shows 3D spin configurations in the cylindrical wire from the analysis of the local magnetization (M_x, M_y, and M_z). The sectional spin structures in the BP-DW region are visualized in the insets. The BP is clearly observed at the DW center between two vortex cores pointing opposite to each other.

Varying the magnetic field from 5 to 150 mT along the nanowire axis ($+x$ direction), the dynamic behaviors of field-dependent BP-DW propagation were investigated. The BP-DW position was defined by

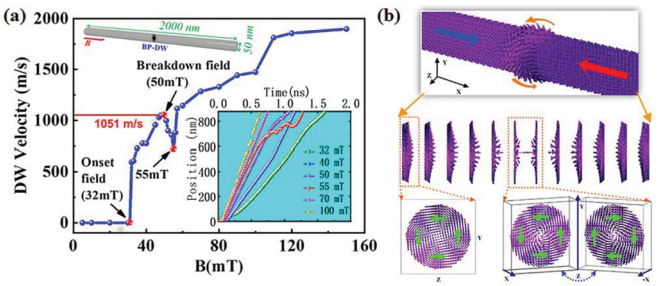

FIG. 1. (a) The average BP-DW velocity with respect to the field strength. The schematic inset shows geometry and dimension of the cylindrical nanowire, and the color background inset graph shows the time-dependent DW position under external fields of 32, 40, 50, 55, 70, and 100 mT. (b) 3D spin structures in the BP-DW region in cylindrical wire. Spin configurations are sectionally visualized by analyzing the local magnetization (Mx, My, and Mz). The green arrows schematically represent spin directions.

the center position of the DW region considering that BP may be annihilated in the cylindrical nanowire. As shown in Fig. 1(a), the DW cannot move until the external field strength is strong enough ($\geq$32 mT) to overcome the intrinsic pinning,[20] and then the average BP-DW velocity gradually increases with respect to the increase in the external field strength. Very interestingly, it is observed that there exists an abrupt decrease in the average BP-DW velocity after B = 50 mT, which is a similar behavior as the Walker breakdown in the 2D wire case. Although the field strength increases, the velocity of the BP-DW propagation is abruptly slowed, from ~1051 m/s at 50 mT down to ~724 m/s at 55 mT. After 55 mT, the BP-DW velocity rapidly recovers, and at 57 mT, the velocity has reached again its original level at 50 mT. The time-dependent position for each field case is plotted in the color-background inset of Fig. 1(a), where a rather complex profile is clearly observed in the case of 55 mT where the DW velocity does not increase monotonously with the field as in other cases. Note that a rather uniform motion trend is restored for the fields stronger than the breakdown field (see the cases of 70 mT and 100 mT), while the average velocity of the BP-DW tends to reach a maximum value of ~2000 m/s for the field stronger than 110 mT due to the intrinsic reversal time of the BP spin texture.[20]

To further investigate the observed BP-DW breakdown phenomenon in detail, the changes of curling spin structures in the BP-DW region are examined before the breakdown occurs for the spins satisfying $|M_x/M_s| \leqslant 0.1$. Since the DW center structure of curved spins looks like a cone lying horizontally in the direction of the external field (see the dark green arrows in the inset of Fig. 2) and it is found that the opening angle of the cone-like structure is sensitive to the field strength, the variation of the average half opening angle ($\bar{\theta}$) is investigated intensively. The $\bar{\theta}$ value is determined as follows: $\bar{\theta} = \frac{1}{n}\sum_{i=n} \tan^{-1}(|y_i - y_{BP}|/|x_i - x_{BP}|)$ for each spin inside the DW conical structure, where (x_{BP}, y_{BP}) and (x_i, y_i) $(i = 1, 2, \cdots, n)$ are coordinate positions of the BP and spins in the DW conical structure, respectively. As shown in Fig. 2, the value of $\bar{\theta}$ decreases with the increasing field strength. Driven by the field with given strength, from the overall profile of $\bar{\theta}$, it is found that the angle is almost constant despite some perturbations, except for the case of 55 mT. In the case of 55 mT, $\bar{\theta}$ is observed to increase gradually over time until the breakdown occurs, as illustrated in Fig. 2(c). It is noteworthy that the $\bar{\theta}$ perturbations occur, implying that there could be SW excitation during the BP-DW motion as a way to release accumulated exchange energy. According to our previous work, the BP motion can be attributed to the exchange drag action on the BP core by the surrounding curling spin structure, thereby releasing the exchange energy accumulated in the BP-DW.[20] The interaction between the motion of the BP and the curling spin structure in the cylindrical nanowire causes the change of the DW structure and eventually leads to a structural collapse of the BP-DW due to an excessive accumulation of exchange energy. This means that the BP-DW structure changes to a metastable spin structure [3D transverse-DW-like helical spin structure, see the $t = 0.78$ ns snapshot in Fig. 3(b)]. Moreover, the change of the DW structure can also excite a Cherenkov-type SW emission[10,50] and then propagation[52] in the nanowire during the BP-DW propagation, which could possibly trigger the BP-DW breakdown phenomenon.

To confirm our inference, the real-time distribution of the normalized z-component magnetization (M_z/M_s) in the xz-plane at $y = 25$ nm is intensively examined under the 55-mT field. Snapshots taken at 0.19, 0.59, 0.67, 0.74, and 0.78 ns are shown in Fig. 3(a). At $t = 0.19$ ns, an asymmetric structure of the BP-DW is observed due to the action of the external field, where there is no obvious SW around

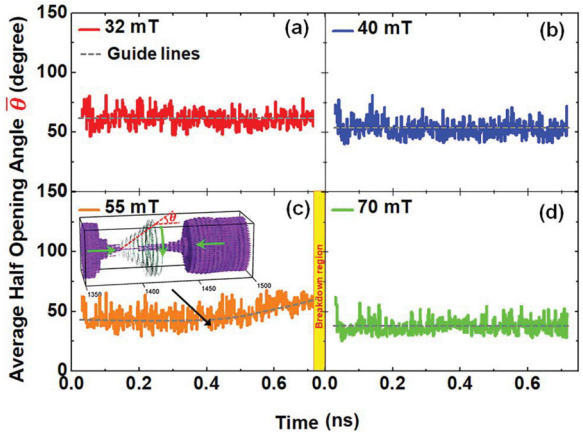

FIG. 2. The average half opening angle $\bar{\theta}$ of the conical spin structure in the asymmetric BP-DW changes over time under (a) 32 mT, (b) 40 mT, (c) 55 mT, and (d) 70 mT. The inset shows a snapshot for the BP-DW spin configurations of $|M_x/M_s| \leqslant 0.1$ and $|M_x/M_s| \geqslant 0.99$ under 55 mT. The green arrows schematically represent spin directions.

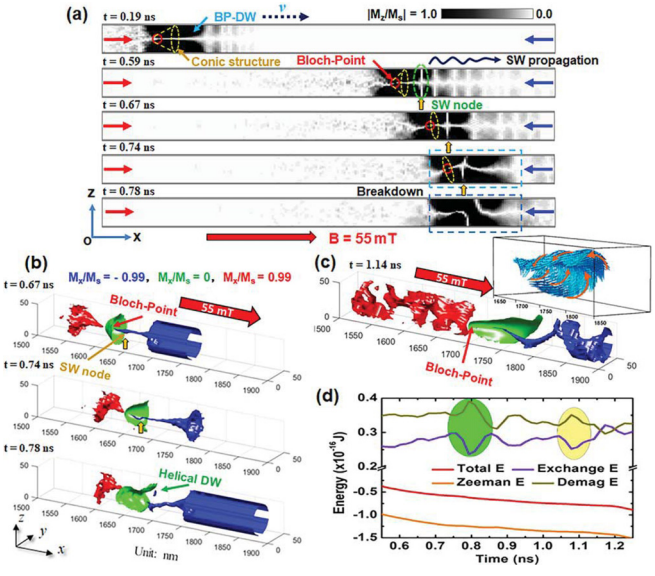

FIG. 3. Snapshots of $|M_z/M_s|$ component magnetization distribution at (a) $t = 0.19$, $t = 0.59$, $t = 0.67$, $t = 0.74$, and $t = 0.78$ ns under 55 mT. The gray code represents the z-component normalized magnetization distribution on the xz-plane. The red and blue arrows indicate the direction of magnetic domain magnetization on both sides of the DW. (b) Side sectional view of the detailed BP spin structure corresponding to the dotted region of (a) at $t = 0.67$ ns, $t = 0.74$ ns, and $t = 0.78$ ns. (c) Side sectional view of the detailed circling spin structure and the detailed BP spin structure at $t = 1.14$ ns for the reframed BP-DW. The red, green, and blue color isosurfaces indicate the spin configurations satisfying $M_x/M_S = -0.99$, $M_x/M_S = 0$, and $M_x/M_S = 0.99$, respectively. (d) Profiles of various magnetic energies over the time in the breakdown region.

it. With the rapid movement of the BP-DW along the wire axis, it is found that the BP-DW structure is gradually changing. This is attributed to the fact that velocity of the DW conical structure is gradually reduced due to the influence of the SW generated in front of the DW. Comparing the BP-DW width and the spacing between SW nodes in the snapshots at $t = 0.59$ ns and 0.67 ns, it is observed that the compression of the BP-DW structure is due to the SW. It is interesting to note that the change or even collapse of the BP-DW structure is accompanied when the BP tries to surpass the conical spin structure of the BP-DW, as schematically shown by the yellow dotted lines in Fig. 3(a). At $t = 0.67$ and 0.74 ns, the conical spin structure of the BP-DW begins to tilt and deform under the influence of the SW, and the position of the SW node near the BP also deviates from the central axis of the nanowire (see the positions indicated by the yellow solid arrows). From the snapshots at $t = 0.74$ and 0.78 ns, it is observed that the BP-DW spin structure has begun to deform and collapse, where, instead of moving forward along the direction of the driving field, the DW exhibits a typical breakdown behavior. Before the breakdown, the instantaneous velocity of the DW reaches a critical value (~1085 m/s) under the 55-mT field,[10,50] which is close to the propagating velocity (~1177 m/s) of the excited SW excited by the DW in this wire (see Fig. 4), clearly showing a SW excitation by the change of the BP-DW conical structure (the θ perturbations). An average time of ~3.7 ps is needed to reverse the spin structure in the BP during the BP-DW propagation with ~1085 m/s before the breakdown. As demonstrated in the snapshots, there is an interaction between the BP-DW and the front SW, analogous to the spin-Cherenkov effect.[10,50,51]

The inner spin structures of the BP-DW at $t = 0.67$, 0.74, and 0.78 ns are illustrated in Fig. 3(b) where the spins satisfy $M_x/M_s = -0.99, M_x/M_s = 0$, and $M_x/M_s = 0.99$, which are indicated by red, green, and blue color isosurfaces, respectively. At $t = 0.67$ ns, it is observed that the SW node next to the BP-DW is located at the central axis of nanowire (see the yellow solid arrow), and the conical spin structure around the BP maintains an axisymmetric structure (see the green isosurface). At $t = 0.74$ ns, the position of the SW node deviates from the central axis [see the snapshot of Fig. 3(a)], and the structural symmetry of the BP-DW is broken (see the yellow solid arrow), which inevitably results in the deformation of the BP-DW conical structure. As depicted by the green isosurface in the snapshots, the BP-DW conical structure begins to deform from one side and completely collapses at $t = 0.78$ ns. As $t = 0.78$ ns, no BP is observed, and an unstable 3D transverse-DW-like helical spin structure is formed[53,54] (see the green isosurface in this snapshot). In the process of forming the helical spin structure, it is found that the DW stops moving forward, and the SW formed in front of the DW disappears as well [see the dotted box area in Fig. 3(a)]. Interestingly, a helical spin structure appears briefly in the nanowire when the DWs collapse. After the helical spin structure rotates one period around the center axis of the nanowire (see the supplementary material), a BP-DW is re-formed with the same chirality as the original DW [see Fig. 3(c)]. From an energy point of view, the counterclockwise curling spin structure with respect to the direction of the applied field is more stable than the clockwise structure,[10,55] which thanks to a chirality symmetry breaking. The change in magnetic energies during the DW propagation is plotted, as illustrated in Fig. 3(d). The total magnetic energy and the Zeeman energy decrease gradually in the process of DW propagation. The exchange energy competes with the demagnetizing energy, especially in the BP-DW breakdown region. When the adjacent SW node approaches slowly the BP, the exchange energy increases (the violet line), but the demagnetizing energy does not significantly change (the dark yellow line), until the BP moves out of the nanowire. At $t = 0.78$ ns, the exchange energy suddenly decreases to a minimum, whereas the demagnetizing energy increases to a maximum, corresponding to the moment when the BP moves out of the nanowire (see the green colored area). During the process of the helical DW formation, the exchange energy as well as the demagnetizing energy undergoes an unstable transitional state with some energy fluctuations. Around $t = 1.07$ ns, the exchange energy and the demagnetizing energy compete with each other again (see the dark yellow colored area), as a new BP-DW with a counterclockwise curling spin structure is formed.

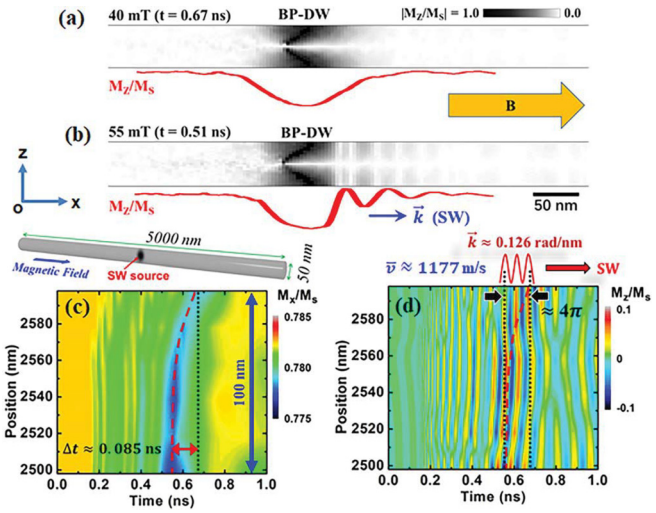

FIG. 4. Snapshots of the $|M_z/M_s|$ distribution at (a) $t = 0.67$ ns under 40 mT and (b) $t = 0.51$ ns under the 55 mT field in 2 μ m cylindrical nanowire. The gray code represents the $|M_z/M_s|$ distribution on the *xz*-plane. Two red curves represent the spatial distribution of M_z/M_s around the BP-DW along the x-axis. The top of (c) is a 5-μm long cylindrical nanowire. Changes in (c) M_x/M_s and (d) M_z/M_s over the time in each cell on the centerline of the nanowire along the *x*-axis. The red arrow in (d) represents the propagating direction of SWs. Color codes represent M_x/M_s and M_z/M_s. The dotted red line guides the path of the SW propagation through two cycles (4π).

To confirm the existence of the Cherenkov-type breakdown, it is important to determine the propagation velocity of the SW phase; however, it is very difficult to accurately determine the velocity of the SW phase due to the complex changes of the DW structure and the edge effect comes from the wire ends during the BP-DW (as a moving SW source) propagation. As shown in Fig. 4(a), when the BP-DW velocity is lower than a critical velocity [$v_0 \approx 1050$ m/s in our case, see Fig. 1(a)], the DW hardly excites any Cherenkov-type SWs.[51] Cherenkov-type SWs have been observed when the BP-DW velocity is larger than v_0, which are excited by the DW and rapidly attenuated in the DW front, as shown in Fig. 4(b). To determine more accurately the minimum velocity and the effective length of SW phase propagation under the 55-mT driving field, a micromagnetic simulation is performed by changing the length of the cylindrical nanowire (5-μm), since the SW dispersion relation in magnetic media is not restricted by

particular geometries,[51] as shown in the inset at the top of Fig. 4(c). Once a SW is generated from the center of nanowire, it propagates asymmetrically along the wire axis direction ($-x$ and $+x$). The wavelength (λ) of the generated SW propagating along the $+x$-axis (right direction) is larger than that along the $-x$-axis (left direction). Interestingly, a SW phase propagating asymmetrically along the $+x$-axis is observed. The variation of the M_x-component of each cell at the center axis of the nanowire is shown in Fig. 4(c). It is found that a shock-wave-like SW phase propagates about 100 nm along the $+x$-axis with an average velocity of ~1177 m/s ($>v_0$) and then disappears gradually, as indicated by the dotted red guided line in Fig. 4(c). This average velocity of the SW phase in the cylindrical nanowire is similar to the phase velocity of $v_p \approx 1200$ m/s of SWs in a flat Permalloy nanowire (see Ref. 51). In the present case, the BP-DW acts as a moving SW source. The SW is excited spontaneously from the DW as soon as its velocity is higher than the minimum SW phase velocity.[10] Under the 55-mT field, the SW phase velocity becomes very close to the instantaneous velocity of ~1085 m/s of the BP-DW before the breakdown, and the wave vector $k = 2\pi/\lambda$ is ~0.126 rad/nm [see Fig. 4(d)], which is very close to the value of $k \approx 0.125$ rad/nm reported in Ref. 51. This means that the Cherenkov-type breakdown as a resonance effect occurs instantaneously when the velocity of the moving SW source (DW) exceeds the phase velocity of the SW, and therefore, there is an inevitable correlation between the velocity of the wave source (1050 m/s) and the wave vector ($k = 0.125$). We conclude that the interaction between the spontaneously emitting SW and the BP-DW is the key to the 3D DW breakdown behavior in a cylindrical ferromagnetic wire.

In conclusion, a Cherenkov-type breakdown behavior during the BP-DW propagation was investigated in the cylindrical nanowire with the varying magnetic field strength. When the BP velocity is close to the critical SW phase velocity, a BP-DW breakdown phenomenon is observed due to the interaction between the spontaneously emitting SW and the BP-DW. The existence of the Cherenkov-type 3D breakdown phenomenon and the intrinsic speed limit of BP-DW should be considered for the future development of spintronic devices based on 3D spin texture. In addition, the BP-DW as a 3D spin texture can shield magnetic flux leakage and has intrinsic pinning behavior in cylindrical nanowires, which could be beneficial for the design and integration of spintronic devices based on DW motion without an artificial pinning site.

See the supplementary material for the "spiral propagation" behavior of the 3D transverse-DW-like helical spin structure in the cylindrical nanowire.

AUTHORS' CONTRIBUTIONS

X.-P.M. and J.Z. contributed equally to this work.

This work was supported by the National Natural Science Foundation of China (Grant No. 11474183), the Korea Research Foundation (NRF) (Grant No. 2018R1A2B3009569), and the Korea Basic Science Institute (KBSI) (Grant No. D39614). This work was also supported by the National Key R&D Program of China (Grant Nos. 2017YFB0903700 and 2017YFB0903702), the YiChang Government Funding (Grant No. A19-402-a05), and Yichang Key Laboratory of Magnetic Functional Materials. P.F. acknowledges support by the U.S. Department of Energy, Office of Science, Office of Basic Energy Sciences, Materials Sciences and Engineering Division under Contract No. DE-AC02-05-CH11231 (NEMM program MSMAG).

DATA AVAILABILITY

The data that support the findings of this study are available within this article and its supplementary material or from the corresponding author upon reasonable request.

REFERENCES

[1]C. Donnelly, M. Guizar-Sicairos, V. Scagnoli, S. Gliga, M. Holler, J. Raabe, and L. J. Heyderman, Nature **547**, 328 (2017).
[2]A. Fernández-Pacheco, R. Streubel, O. Fruchart, R. Hertel, P. Fischer, and R. P. Cowburn, Nat. Commun. **8**, 15756 (2017).
[3]P. Fischer, D. Sanz-Hernández, R. Streubel, and A. Fernández-Pacheco, APL Mater. **8**, 010701 (2020).
[4]C. Blanco-Roldán, C. Quirós, A. Sorrentino, A. Hierro-Rodríguez, L. M. Álvarez-Prado, R. Valcárcel, M. Duch, N. Torras, J. Esteve, J. I. Martín, M. Vélez, J. M. Alameda, E. Pereiro, and S. Ferrer, Nat. Commun. **6**, 8196 (2015).
[5]Y. Zhou, E. Iacocca, A. A. Awad, R. K. Dumas, F. C. Zhang, H. B. Braun, and J. Åkerman, Nat. Commun. **6**, 8193 (2015).
[6]J. Sampaio, V. Cros, S. Rohart, A. Thiaville, and A. Fert, Nat. Nanotechnol. **8**, 839 (2013).
[7]S. Rohart, J. Miltat, and A. Thiaville, Phys. Rev. B **93**, 214412 (2016).
[8]S. K. Kim and O. Tchernyshyov, Phys. Rev. B **88**, 174402 (2013).
[9]C. Andreas, A. Kákay, and R. Hertel, Phys. Rev. B **89**, 134403 (2014).
[10]R. Hertel, J. Phys.: Condens. Matter **28**, 483002 (2016).
[11]F. Zheng, F. N. Rybakov, A. B. Borisov, D. Song, S. Wang, Z. A. Li, H. Du, N. S. Kiselev, J. Caron, A. Kovács, M. Tian, Y. Zhang, S. Blügel, and R. E. Dunin-Borkowski, Nat. Nanotechnol. **13**, 451 (2018).
[12]J. Stöhr and J. C. Siegmann, *Magnetism: From Fundamentals to Nanoscale Dynamics* (Springer-Verlag, Berlin, 2006).
[13]D.-Y. Kim, M.-H. Park, Y.-K. Park, J.-S. Kim, Y.-S. Nam, D.-H. Kim, S.-G. Je, H.-C. Choi, B.-C. Min, and S.-B. Choe, NPG Asia Mater. **10**(1), e464 (2018).
[14]H. Forster, T. Schrefl, D. Suess, W. Scholz, V. Tsiantos, R. Dittrich, and J. Fidler, J. Appl. Phys. **91**, 6914 (2002).
[15]H. Forster, T. Schrefl, W. Scholz, D. Suessa, V. Tsiantosa, and J. Fidler, J. Magn. Magn. Mater. **249**, 181 (2002).
[16]R. Hertel, J. Magn. Magn. Mater. **249**, 251 (2002).
[17]W. Scholz, H. Forster, D. Suess, T. Schrefl, and J. Fidler, Comput. Mater. Sci. **25**, 540 (2002).
[18]R. Hertel and J. Kirschner, Physica B **343**, 206 (2004).
[19]R. Wieser, U. Nowak, and K. D. Usadel, Phys. Rev. B **69**, 064401 (2004).
[20]H.-G. Piao, J.-H. Shim, D. Djuhana, and D.-H. Kim, Appl. Phys. Lett. **102**, 112405 (2013).
[21]M. Vázquez, *Magnetic Nano- and Microwires, Design, Synthesis, Properties and Applications*, 2nd ed. (Woodhead Publishing, 2020).
[22]D. Djuhana, H.-G. Piao, S.-C. Yu, S. K. Oh, and D.-H. Kim, J. Appl. Phys. **106**, 103926 (2009).
[23]T. Ono, H. Miyajima, K. Shigeto, K. Mibu, N. Hosoito, and T. Shinjo, Science **284**, 468 (1999).
[24]D. Atkinson, D. A. Allwood1, G. Xiong, M. D. Cooke, C. C. Faulkner, and R. P. Cowburn, Nat. Mater. **2**, 85 (2003).
[25]G. S. D. Beach, C. Nistor, C. Knutson, M. Tsoi, and J. L. Erskine, Nat. Mater. **4**, 741 (2005).
[26]C.-Y. You, Appl. Phys. Lett. **92**, 152507 (2008); **92**, 192514 (2008).
[27]H.-G. Piao, J.-H. Shim, S.-H. Lee, D. Djuhana, S. K. Oh, S.-C. Yu, and D.-H. Kim, IEEE Trans. Magn. **45**, 3926 (2009).
[28]J.-S. Kim, M. A. Mawass, A. Bisig, B. Krüger, R. M. Reeve, T. Schulz, F. Büttner, J. Yoon, C.-Y. You, M. Weigand, H. Stoll, G. Schütz, H. J. M. Swagten, B. Koopmans, S. Eisebitt, and M. Kläui, Nat. Commun. **5**, 3429 (2014).
[29]C. Chen, H.-G. Piao, J.-H. Shim, L.-Q. Pan, and D.-H. Kim, Chin. Phys. Lett. **32**, 087502 (2015).

[30]S. S. P. Parkin, U.S. patent 6,834,005 (2004); S. S. P. Parkin, M. Hayashi, and L. Thomas, Science **320**, 190 (2008).
[31]R. Moriya, L. Thomas, M. Hayashi, Y. B. Bazaliy, C. Rettner, and S. S. P. Parkin, Nature **4**, 368 (2008); M. Hayashi, L. Thomas, R. Moriya, C. Rettner, and S. S. P. Parkin, Science **320**, 209 (2008).
[32]E. Saitoh, H. Miyajima, T. Yamaoka, and G. Tatara, Nature **432**, 203 (2004).
[33]M. Kläui, M. Laufenberg, L. Heyne, D. Backes, U. Rüdiger, C. A. F. Vaz, J. A. C. Bland, L. J. Heyderman, S. Cherifi, A. Locatelli, T. O. Mentes, and L. Aballe, Appl. Phys. Lett. **88**, 232507 (2006).
[34]M. Hayashi, L. Thomas, C. Rettner, R. Moriya, Y. B. Bazaliy, and S. S. P. Parkin, Phys. Rev. Lett. **98**, 037204 (2007).
[35]G. Meier, M. Bolte, R. Eiselt, B. Krüger, D.-H. Kim, and P. Fischer, Phys. Rev. Lett. **98**, 187202 (2007).
[36]D.-S. Han, S.-K. Kim, J.-Y. Lee, S. J. Hermsoerfer, H. Schutheiss, B. Leven, and B. Hillebrands, Appl. Phys. Lett. **94**, 112502 (2009).
[37]S.-M. Seo, H.-W. Lee, H. Kohno, and K.-J. Lee, Appl. Phys. Lett. **98**, 012514 (2011).
[38]X. S. Wang, P. Yan, Y. H. Shen, G. E. W. Bauer, and X. R. Wang, Phys. Rev. Lett. **109**, 167209 (2012).
[39]A. V. Khvalkovskiy, V. Cros, D. Apalkov, V. Nikitin, M. Krounbi, K. A. Zvezdin, A. Anane, J. Grollier, and A. Fert, Phys. Rev. B **87**, 020402(R) (2013).
[40]S. Emori, U. Bauer, S.-M. Ahn, E. Martinez, and G. S. D. Beach, Nat. Mater. **12**, 611 (2013).
[41]N. L. Schryer and L. R. Walker, J. Appl. Phys. **45**, 5406 (1974).
[42]F. H. de Leeuw, R. v den Doel, and U. Enz, Rep. Prog. Phys. **43**, 689 (1980).
[43]M. Yan, A. Kákay, S. Gliga, and R. Hertel, Phys. Rev. Lett. **104**, 057201 (2010).
[44]N. D. Mermin, Rev. Mod. Phys. **51**, 591 (1979).
[45]S. Da Col, S. Jamet, N. Rougemaille, A. Locatelli, T. O. Mentes, B. Santos Burgos, R. Afid, M. Darques, L. Cagnon, J. C. Toussaint, and O. Fruchart, Phys. Rev. B **89**, 180405(R) (2014).
[46]M. J. Donahue and D. G. Porter, see http://math.nist.gov/oommf for "OOMMF User's Guide (2002)."
[47]A. Vansteenkiste, J. Leliaert, M. Dvornik, M. Helsen, F. Garcia-Sanchez, and B. V. Waeyenberge, AIP Adv. **4**, 107133 (2014).
[48]P. Landeros and Á. S. Núñez, J. Appl. Phys. **108**, 033917 (2010).
[49]J. A. Otálora, J. A. López-López, P. Vargas, and P. Landeros, Appl. Phys. Lett. **100**, 072407 (2012).
[50]M. Yan, C. Andreas, A. Kákay, F. García-Sánchez, and R. Hertel, Appl. Phys. Lett. **99**, 122505 (2011).
[51]M. Yan, A. Kákay, C. Andreas, and R. Hertel, Phys. Rev. B **88**, 220412(R) (2013).
[52]H.-G. Piao, J.-H. Shim, M. Yang, L. Pan, and D.-H. Kim, IEEE Trans. Magn. **51**, 7100706 (2015).
[53]M. C. Sekhar, H. F. Liew, I. Purnama, W. S. Lew, M. Tran, and G. C. Han, Appl. Phys. Lett. **101**, 152406 (2012).
[54]D. W. Wong, M. C. Sekhar, W. L. Gan, I. Purnama, and W. S. Lew, J. Appl. Phys. **117**, 17A747 (2015).
[55]M. Yan, C. Andreas, A. Kákay, F. García-Sánchez, and R. Hertel, Appl. Phys. Lett. **100**, 252401 (2012).